Vertical Thermal O^+ Flows at 850 km in Dynamic Auroral Boundary Coordinates

R.J. Redmon[1], W.K. Peterson[2], L. Andersson[2], E.A. Kihn[1], W.F. Denig[1], M. Hairston[3], R. Coley[3]

[1]National Oceanic Atmospheric Administration, National Geophysical Data Center, Boulder, CO.

[2]Laboratory for Atmospheric and Space Plasmas, University of Colorado, Boulder, CO.

[3]Center for Space Sciences, University of Texas at Dallas, Richardson, TX.

Contemporary magnetosphere models now include species dependent dynamics. Energetic O^+ has significant consequences for the energy stored in the ring current, the rate of reconnection, and perhaps the timing of substorm injections. The mechanism by which thermal O^+ escapes from the top of the ionosphere and into the magnetosphere is not fully understood. Previous studies have used dynamic auroral boundary coordinates to describe the outflowing energetic O^+ ions above the ionosphere. In this study we focus on the vertical flow of O^+ ions at lower altitudes before they are accelerated to escape velocity. An algorithm has been devised to identify auroral zone boundaries using precipitating electron observations from the Defense Meteorological Satellite Program (DMSP) spacecraft. Vertical ion

flows measured by the DMSP Special Sensor for Ions Electrons and Scintillation (SSIES) Ion Drift Meter (IDM) and the Retarding Potential Analyzer (RPA) instruments aboard the F12 (noon-midnight) and F13 (dawn-dusk) spacecraft from 1997-1998 were projected into dynamic auroral boundary coordinates and used to investigate the dependence of southern hemisphere bulk flows on Interplanetary Magnetic Field (IMF) and geomagnetic conditions. Initial results show that 1) net upward flows occur primarily in the auroral zone and net downward flows occur primarily in the polar cap, 2) there exists a strong upward flow at 9 Magnetic Local Time (MLT) near the polar cap boundary, 3) the downward ion flow orientation is strongly dependent on IMF By, and 4) the auroral boundary does not coincide exactly with the upward/downward boundary for bulk flows.

1. Introduction

Since the discovery of heavy ions in the inner magnetosphere during a geomagnetic storm (Shelley et al., 1972) it has been suggested that ionospheric outflows can supply the entire magnetospheric ion population (Chappel et al., 1987). Attempts have been made to describe the contribution of ionospheric plasma to the magnetosphere under varying solar

and magnetic conditions. For a summary of this research see Moore and Horwitz (2007), and Yau et al., (2007).

Low altitude ionospheric ions are produced predominantly through photoionization and then heated and driven up magnetic field lines. This results in an upward bulk flow of plasma. Most of the upward population does not have escape energy and returns to the ionosphere. Some of the upward flowing ions are energized or accelerated to escape velocities and transported to the plasma sheet. Most energization and acceleration processes occur in the auroral oval where soft precipitation, parallel electric fields and wave activities are common (Gorney et al., 1981, Yau and Andre, 1997). At low altitudes, Joule heating and soft precipitation dominate. At high altitudes, parallel electric fields, plasma waves, gradient magnetic field convection, and induced centrifugal forces provide acceleration. Auroral heating and ion acceleration are fairly well studied (Andre and Yau, 1997; Strangeway et al., 2005), but the efficiency of this coupling is still unclear. Significant deposition of energy into the ionosphere by precipitating particles should increase upward flows on coincident flux tubes. However it is uncertain whether regions of peak non-escaping flows are collocated with the regions of strongest acceleration.

Contemporary magnetosphere modelers are now including species dependent dynamics in their magneto-hydrodynamic (MHD) models and have shown that energetic O^+ has significant consequences for the ring current stored energy (Lotko, 2007), the rate of reconnection (Shay and Swisdak, 2004), and perhaps the timing of substorm injections (Peterson et al., 2002). Most MHD models have an inner boundary at 2-3 Re and are connected to the ionosphere through various assumptions about Magnetosphere-Ionosphere (MI) coupling. Recent models attempted to include large-scale H^+ and O^+ outflow flux rates (Winglee et al., 2002). The coupling of upward flowing ions at low altitude to acceleration mechanisms at altitudes of 2-3 Re is not well understood and motivates further investigation.

Past researchers have described large-scale vertical bulk ion flows observed by the Dynamics Explorer (Loranc et al., 1991) and Defense Meteorological Satellite Program (DMSP) (dawn-dusk only) (Coley et al., 2003) and accelerated ion outflow features observed by the Fast Auroral SnapshoT (FAST) (Andersson et al., 2004; Andersson et al., 2005), Akebono (Cully et al. 2003), and POLAR (Peterson et al., 2006; Su et al., 1998) spacecraft. Recently, Andersson et al. (2004) and Peterson et al. (2008) have developed and employed a technique to express, in dynamic auroral boundary related coordinates, outflows with energy exceeding 3eV collected from FAST and

outflows with energy exceeding 15eV collected from POLAR. This technique works well to mitigate ambiguities associated with the expansion and contraction of the auroral oval and provides outflow values in a coordinate system compatible with magnetospheric model inputs. However, the FAST and POLAR results are for escaping ions and thus their results are for ions that have already been accelerated.

Bulk flows at 850 km, which factor into the total budget of ions available for acceleration at higher altitudes, are the focus of this study. The same dynamic auroral boundary coordinate philosophy (Anderson et al., 2004; Peterson et al., 2008) has been applied and an automated technique has been developed to select appropriate auroral zone boundaries for each DMSP polar crossing. Using this new coordinate system, vertical ion flows have been calculated for southern hemisphere crossings of the DMSP F12 (noon-midnight) and F13 (dawn-dusk) spacecraft during 1997 and 1998, and the dependence of the bulk flow on Interplanetary Magnetic Field (IMF) conditions and geomagnetic activity levels has been investigated.

This paper presents the first large-scale survey of heavy ion bulk flows measured by DMSP in dynamic auroral boundary coordinates. The data set used and the method of determining dynamic boundaries are described in section 2. Statistical maps of southern hemisphere vertical flows organized

by the planetary magnetic activity index, Kp, and IMF *By* are presented in section 3. A summary of our findings is presented in section 4.

2. Dataset Preparation

To prepare averages of vertical flows observed by the DMSP satellites, a 3-step procedure was adopted. First, the location of the auroral oval was identified using average precipitating electron energy fluxes ($eV/cm^2/s/sr/eV$) observed by the DMSP Special Sensor J4 (SSJ4) instrument. Then the bulk O^+ flow was derived from net ion flow velocities and densities from the DMSP Special Sensor for Ions Electrons and Scintillation (SSIES) Ion Drift Meter (IDM) (Rich and Hairston, 1994) and the Retarding Potential Analyzer (RPA) (Rich and Hairston, 1994; Greenspan et al., 1986) respectively, and organized with respect to these *in situ* auroral boundaries. After all orbits were processed, statistical distributions were produced. For the present study, average flows were grouped by IMF *By* and by Kp.

DMSP satellites have been observing precipitating particle data using the SSJ package since the early 1970s (Meng and Kroehl, 1977) and ion drift data from the SSIES package since 1987 (Rich and Hairston, 1994). DMSP satellites are polar orbiting, axis stabilized, sun synchronous, retrograde

spacecraft that have a nominal orbital period of 101 minutes, an inclination of 98.9 degrees and an altitude of 850 km. Usually 2 to 4 spacecraft are in orbit at any given time, occupying one of two fixed local times, which are approximately 9-21 LT (local time) and 6-18 LT. Due to the diurnal movement of the magnetic pole in the geodetic frame, a wide swath of magnetic local times is sampled daily. In this present study, the contributions from F12 (9-21 LT) and F13 (6-18 LT) were utilized to yield dawn-dusk and pre-noon – pre-midnight coverage.

2.1 Dynamic Boundaries

The SSJ4 observes downward electron and ion fluxes in 20 energy channels ranging from 30eV to 30keV in the local zenith look direction. Two pairs of electrostatic analyzers are employed for this purpose, one pair for electrons and one for ions. One analyzer in each pair is used for low energy particles and provides 10 logarithmically spaced channels between 30eV and 1 keV. The second analyzer in each pair is used for higher energy particles and provides 10 logarithmically spaced channels between 1 keV and 30 keV. Channels are sampled sequentially with the electron and ion analyzers stepping together, producing 20 channels of electron fluxes and 20 channels of ion fluxes once per second (Hardy et al., 1984).

Existing data sets of auroral boundaries were considered before developing a new algorithm. It was found that the existing DMSP boundaries (Newell et al., 1991; Newell et al., 1996), which are general purpose and attempt to associate precipitation features with auroral forms, were insufficient for our needs. These boundaries use separate algorithms for day and for night, leading to day/night discontinuities, and lack an easily accessible figure of merit. The primary objectives supporting the authors' decision to formulate new boundary identifications were: (1) to find the locations in a consistent way, (2) use a methodology similar to that used on FAST and Polar data, (3) fill in unnecessary data gaps in other boundaries and (4) employ a quality index to aid in filtering out lower quality detections. Therefore a new set of boundary identifications was developed for the explicit purpose of identifying the auroral oval and is based on the work by Newell et al. (1991), Newell et al. (1996), Sotirelis and Newell (2000), Andersson et al. (2004) and Peterson et al. (2006).

The auroral zone is the region where the magnetosphere and ionosphere strongly interact. Auroral boundary identification is strongly dependent on the sensitivity, and energy resolution of the electron and ion detectors. The higher energies sampled by the J4 instrument are unambiguously of magnetospheric origin. It is desirable to choose energy flux channels with high signal-to-noise ratios. We use the highest 9 energy channels, with

energies between 1.39 keV and 30 keV, inclusive. Low counts, and/or background signals from penetrating radiation belt particles make detection of the equatorward edge of the auroral zone difficult. An algorithm developed by the Air Force Research Lab (AFRL) has been applied to remove this background noise and an example is displayed for electrons in Figure 1.

A DMSP F12 south polar crossing on January 10, 1997 is presented in Figure 2 as an example of auroral boundary identification. Panels a) and b) show the spectrogram for electrons and ions, respectively. Our automated algorithm identifies four auroral zone crossings on each high latitude pass of a DMSP satellite. This approach has several steps. First, the 9 precipitating electron channels between 1.39 keV and 30 keV are averaged at each observation time. This 1-second average energy flux of precipitating electrons is then smoothed over 30 seconds (Figure 2, panel g). The auroral zone equatorward boundary is identified as the most equatorward region with an appreciable energy flux. The polar cap, i.e. open field lines, is identified as a significant region of depleted precipitating energy flux near the highest latitudes reached by the DSMP satellite.

Identification of the polar cap boundary is complicated due to short duration but significant regions of precipitation such as transpolar arcs (e.g. theta aurora, Peterson and Shelley, 1984). To address this issue, a threshold value

of $10^{4.5}$ eV/cm^2/s/sr/eV was chosen after extensive semi-blind comparisons of 200 randomly chosen orbits. All candidate precipitation regions of time were identified where the spacecraft was above 58 degrees magnetic latitude and the smoothed energy flux of precipitating particles exceeded the given threshold. In each high latitude pass, the flux threshold is exceeded in N regions, where N is most typically 2 and rarely exceeds 3 for the orbits used to create the statistical maps in section 3. These N regions are organized into N*(N-1)/2 pairs and the following dimensionless figure of merit (FOM), which emphasizes feature intensity and separation, is computed for each pair:

$$FOM_{i,j} = A_i/A_{max} + A_j/A_{max} + DT_{i,j}/20$$

The range of computed FOM's is between 0 and 3 and the peak of the distribution is ~1.7. A_i is the total average energy flux summed over the time period of the i-th region, A_{max} is the total average energy flux for the region of maximum average energy flux and $DT_{i,j}$ is the time in minutes spanned between the poleward edge of the i-th region and the poleward edge of the j-th region. DT is divided by 20 minutes, as it is the typical high latitude passage time. This FOM isolates occasional, short duration but strong precipitating energy fluxes characteristic of theta aurora and auroral patches often found within the polar cap. The polar cap is then recorded as the region separated by the poleward edges of the i-th and j-th regions, which maximized our FOM. The equatorward boundary of the auroral zone is

separately determined to be the equatorward edges of the 2 lowest latitude regions (Figure 2, leftmost and rightmost black, dashed, vertical lines). Our algorithm unambiguously locates the polar cap when other methods, which look at the ascending and descending phase of the orbit separately, cannot. Figure 2 presents an example application of the complete technique to an F12 south polar crossing on January 10, 1997 and the vertical dashed lines indicate the resulting choice of auroral zone and polar cap. The choice of suitable equatorward and poleward auroral boundaries results in 3 regimes for organizing *in situ* observations: (1) low latitude (LL), or equatorward of the auroral zone, (2) inside the auroral zone (AZ) and (3) inside the polar cap (PC).

This boundary detection algorithm was applied to all southern hemisphere DMSP F12 and F13 passes in 1997 and 1998 and filtered for FOM's > 1.7, a number which was qualitatively determined to produce the minimum of spurious boundaries, while maintaining a significant dataset. In the interval examined there were 10,220 DMSP orbits for each of F12 and F13, for a total of 20,440 potential southern hemisphere crossings. After filtering for a FOM > 1.7, there were 9,386 remaining crossings (or 46%) and Figure 3 illustrates the location of the 18,772 boundaries our algorithm identified for each of the equatorward edge (left) and the poleward edge (right) of the auroral zone. The results are displayed in sun fixed magnetic coordinates,

for various levels of geomagnetic activity. The combination of DMSP F12 and F13 provides reasonable coverage for the magnetic local times between 3 and 9 hours and between 17 and 24 hours. The equatorward edge of our auroral zone descends in latitude as Kp increases for all of these local times. The polar cap boundary shows less systematic migration with Kp for low to moderate activity, with signs of equatorward movement in pre-noon and pre-dusk sectors for high activity. In comparison to the John's Hopkins University Applied Physics Laboratory (JHUAPL) technique, the new technique uses the same algorithm for day and night MLTs and produces an easily accessible figure of merit. These new boundaries agree with the JHUAPL boundaries reasonably well when the latter are available and counts due to penetrating radiation are low.

2.2 Vertical Flows

The DMSP IDM provides the net bulk plasma velocity in 2 orthogonal, cross-track directions, and the RPA provides plasma density on a cadence of 4 seconds. In this paper, the cross-track velocity components are designated as Vy and Vz, where Vz is positive for flows in the upward spacecraft zenith direction and Vy is positive looking to the left of the orbital plane (i.e. positive sunward). The net number flux at each measurement time is derived from the product of the velocity and density. The panels in Figure 2

show an example of the c) bulk ion vertical number flux, d) ion density, e) vertical flow and f) horizontal flow for an F12 south polar crossing on January 10, 1997.

Reliability of the IDM output is directly dependent on the ratio of O^+/H^+. IDM data are most reliable when this ratio is large. An algorithm provided by the Center for Space Sciences, University of Texas at Dallas was used to produce 4 levels of quality: good, caution, poor, and unknown. Only data flagged as "good" have been used in this paper. Since significant vertical drifts are observed primarily in the aurora and polar cap, the Coley et al. (2003) baseline adjustment technique was applied to the vertical drift (Vz) by subtracting a line from Vz such that the median Vz between 50 and 55 magnetic latitude is set to 0. This technique works best for small adjustments. Cases that required adjustments that exceeded 100 m/s have not been used in our investigation. Data from orbits heading into the sun in their descending phase often suffer from sun glint which appears as non physical horizontal and vertical bulk plasma flows for a significant portion of the pass. Data from DMSP/F12 are frequently compromised by sun glint during northern hemisphere. For this reason, and to mitigate local time sampling biases, only southern hemisphere passes for both F12 and F13 were included in this study.

2.3 Boundary Organized Vertical Flows

The method of obtaining statistical maps of net thermal O^+ flow is illustrated in Figure 4. First, auroral zone crossing times were determined as described in section 2.1. These locations were then used to categorize the IDM vertical flows into low latitude, auroral zone and polar cap regions. Hourly IMF *By* from the OMNIWeb data system, and the 3 hourly planetary magnetic activity index Kp were used to categorize each crossing. All passes exceeding a chosen FOM contributed to creating final statistical maps of a chosen net bulk flow parameter (e.g. Vertical velocity (Vz), ion density (Ni), net flux (Vz*Ni)) in a chosen coordinate system. We will now describe the method of projecting a bulk flow parameter into dynamic auroral boundary coordinates. As a crossing passes through the auroral zone, each observation point is mapped latitudinally to its fractional position within the auroral zone or polar cap using the following simple mapping functions for the AZ and the PC respectively:

$$L_{AZ} = (|MLat(t)| - |MLat_{AZ}|) / (|MLat_{PC}| - |MLat_{AZ}|)$$

$$L_{PC} = (|MLat(t)| - |MLat_{PC}|) / (90 - |MLat_{PC}|)$$

$MLat_{AZ}$ and $MLat_{PC}$ are the magnetic latitude equatorward boundaries of the AZ and PC respectively, which were determined in accordance with the method of section 2.1. L_{AZ} and L_{PC} both map their input values between 0 and 1 with 0 equal to the equatorward edge and 1 equal to the poleward

edge of the region in question. Twenty-four bins, centered on magnetic local noon, were used to discretize the local time and ten bins each were used to discretize the latitudinal extent of the AZ and PC respectively. In this manner, we have removed the expansion and contraction of the auroral boundary while maintaining the magnetic local time information, such that observations from crossings with different auroral extents can be statistically combined. In the example of Figure 4, the statistical plot on the left shows net downward O^+ in magnetic coordinates (i.e. no latitudinal normalization), and the plot on the right shows net downward O^+ in dynamic boundary coordinates. Both figures are for IMF *By* < 0 and all Kp. In the figure on the right, the white concentric circle represents the polar cap boundary in dynamic boundary coordinates.

3. Statistical Maps of Vertical flows in Boundary Coordinates

This section presents the first large-scale survey of vertical O^+ fluxes in dynamic boundary coordinates and discusses some initial results. All available orbits in 1997 and 1998 for DMSP F12 and F13 were processed by the technique described in section 2. Due to occasional noise artifacts from sun glints in F12 northern polar crossings, and a desire to maintain reasonable spatial sampling statistics, this investigation is confined to vertical flows in the southern hemisphere. With appropriate symmetry

considerations the results that follow are generally valid for both hemispheres.

The methods we have used are not without their limitations. OMNI hourly IMF By data was used and these hourly averages are biased toward low activity. We have made no correction for the inclination of the magnetic field when interpreting the vertical velocity component of the DMSP/IDM. The angle between the spacecraft zenith and an IGRF derived field is typically less than 17 degrees at the equatorward edge of the auroral zone boundary and this angle decreases as the spacecraft latitude increases and the magnetic inclination increases towards 90 degrees. The most significant source of error from this approach is from the flow of ions in the direction of the spacecraft velocity vector, or ram direction, as these ion flows will contribute to the observed vertical flow. Dawn-dusk orbits (F13) should not be significantly affected by these extraneous flows because the predominant ionosphere flow transverse to the magnetic field is from convective flows and these are also mostly transverse to both the spacecraft motion and the plane of inclination of the magnetic field. Noon-midnight orbits (F12) will be more impacted as the dominant flows transverse to the magnetic field are aligned with the direction of spacecraft motion. In general, these flows will be additive on the noon side and subtractive on the midnight side of the orbit. This bias varies with the sine of the inclination, which is minimized in

the polar cap and greatest at the equatorward edges of the pre-noon and pre-midnight auroral zone. This bias projects nominally less than 14% and 29% of the convecting flows in these local times onto the vertical observations in the PC and AZ respectively, which can be a significant bias during periods of high convection. Finally, the DMSP IDM is insensitive to velocities below ~10 m/s (Coley et al., 2003). Considering that typical densities are on the order of 10^{10} m^{-3}, caution should be used when interpreting fluxes below 10^{11} $m^{-2}s^{-1}$ for all grid cells and when interpreting fluxes below 10^{12} $m^{-2}s^{-1}$ for pre-noon and pre-midnight auroral features.

Figure 5 presents average flows for IMF *By* > 0 and Figure 6 presents flows for *By* < 0. Both figures represent average flows for the southern hemisphere. The results in both figures are organized by flow direction and the planetary activity index Kp. From top to bottom, rows 1-4 represent statistical flows that are organized as 1) upward events, 2) downward events, 3) upward + downward events (highlighting upward), and 4) upward + downward events (highlighting downward). The reader is reminded that the IDM yields the net vertical velocity at each sample time and thus rows 1 and 2 represent those observation times with a net upward and net downward flow respectively. Rows 3 and 4 both represent the sum of 1) upward and 2) downward events. The difference between rows 3 and 4 is that their color bars are oriented to highlight either upward or downward

average flows. Row 5 depicts the total number of samples used. From left to right, columns a) – e) represent Kp ranges, organized as: a) Kp [0-1), b) Kp [1-2), c) Kp [2-3), d) Kp [3-9], e) All Kp. All statistical maps are displayed with the same color scale.

The results in rows 3 and 4 agree with previous observations on DE2 (Loranc et al., 1991) and DMSP (Coley et al., 2003) that the most probable flow direction is downward in the PC and upward in the AZ. Consistent with observations on POLAR/TIDE (Huddleston, 2005) and POLAR/TIMAS (Peterson et al., 2006, 2008), a strong PC upward flow near 9 MLT for all Kp (Figure 5 and 6, rows 1 and 3, all columns) is also observed.

A comparison of rows 2 and 4 for $By > 0$ versus $By < 0$ shows that there is a strong dependence of the location of downward flux in the PC as a function of IMF *By* direction. For $By > 0$, the orientation of downward flow in the southern hemisphere is in a quasi dawn-dusk direction, while the orientation of the downward flow for $By < 0$ is in a quasi noon-midnight direction. To our knowledge, this orientation discrimination of bulk ion downward flow by IMF *By* has not been noted before. It is reasonable to suggest that the pattern results from the orientation of the throat of a typical 2 cell convection pattern in the southern hemisphere for $By > 0$ and for $By < 0$ as depicted in Figure 7. The data in Figure 7 were produced by the Assimilative

Mapping of Ionospheric Electrodynamics (AMIE) (Richmond, 1992). Essentially, the IMF *By* parameter rotates the convection cells and the associated cleft ion fountain (Lockwood et al., 1985), and thus the location of the large-scale net down flowing region in the polar cap. In the southern hemisphere, for $By > 0$, the throat of anti-sunward convection is aligned towards post-dawn hours, whereas for $By < 0$, the throat is aligned towards post-noon. As the pre-noon (cusp) ionosphere is heated, this energy deposition causes ions to flow upward. These upward flowing ions are concurrently undergoing strong anti-sunward convection, through the By rotated throat. A large percentage of this upward flowing population is not energized at higher altitudes, and thus travels a ballistic path as depicted in Figure 8, falling downward under gravity while convecting through the throat toward the nightside. The orientation of this statistical ballistic path is largely independent of Kp for $By > 0$ and somewhat dependent on Kp for $By < 0$. Since the rotation of the throat of convection in the northern hemisphere is also controlled by IMF By but in the opposite sense (Heppner and Maynard, 1987), it is expected that the PC downward fluxes in figures 5 and 6 should relate well to those observed in the northern hemisphere under IMF $By < 0$ and IMF $By > 0$ respectively.

Comparing row 1 in Figures 5 and 6, in the case of $By > 0$, precipitation based boundaries confine most of the upward flowing ions to the AZ,

whereas for *By* < 0, significant upward flowing ions, especially on the dawn side, appear poleward of the PC boundary. This feature is similarly due to the coincident rotation of the throat and cleft ion fountain. Since the auroral zone is the region where the most efficient acceleration mechanisms exist, we infer that under *By* > 0, more ions are available for energization processes.

The following features are also noted in Figures 5 and 6. The net flow of ions for all Kp activity levels [0-9] at pre-midnight local times (MLT 20-24) peaks at the PC edge of the AZ with an upward flux (row 3) that increases with Kp and exceeds $10^{12.5}$ ions/m^2/s during the most disturbed intervals. The net flow of upward ions for moderate to active Kp [2-9] (columns c, d) at post-dusk is enhanced at the AZ equatorial boundary. Nighttime net flux matches or exceeds pre-noon flux. There is a dawn-dusk asymmetry in the filling of the auroral zone with net flux, with the dusk side more uniformly filled. This asymmetry appears to be opposite that of observations on FAST at its higher altitudes (3200-4400 km) (Andersson et al., 2005) and POLAR (Peterson et al., 2008).

Andersson et al., (2005) reported significant dusk O^+ outflow between 1500 and 2500 km and suggested enhanced upward thermal flows as the source. The vertical flows observed by DMSP (Figures 5 and 6, rows 1 and 3) do

show significant upward flows for pre-midnight MLTs. The reader is reminded that the DMSP/IDM observes the net flow for each 4-second sample period. In Figure 8a), we have modeled a hypothetical drifting Maxwellian cold plasma population with a drift speed of 500 m/s and a temperature of 1160 K (or 0.1eV). This drift speed corresponds approximately to low convective flows or active vertical flows in the AZ or near its boundary. The turn around point for active upward flows of 500 m/s is only ~17 km in ~68 seconds. The velocity needed at DMSP to just reach 1500 km with zero remaining kinetic energy is about 3000 m/s and roughly 440 seconds of flight time would have transpired. The hypothetical drifting Maxwellian distribution with a temperature of 1160 K and an upward drift of 500 m/s depicted in Figure 8a) demonstrates that such high bulk flow populations are not probable. Such higher velocity ions would exceed the idealized population's mean drift velocity by 2.3 times the thermal velocity, $V_{thermal}$, where $V_{thermal}$ = sqrt(2kT/m). Also, assuming a moderate convective flow of 1000 m/s, only ~12 degrees would be traversed along a nominal AZ boundary of 70 degrees magnetic latitude. Thus, in order to traverse 5 hours of MLT from DMSP pre-midnight to FAST post-dusk, a similarly improbable transverse flow is required. Therefore, the pre-midnight enhancement of upward flowing ions seen by DMSP cannot explain dusk energetic outflowing ion observations (1500-2500km) using only bulk upward flow + transverse convection on the same flux tubes. Ion energization or acceleration processes must exist

between 850 km and 1500 km in the dusk and/or pre-midnight sector to explain the FAST observations. Comparing upward flowing ions at DMSP with outflowing ions at higher altitudes observed by the FAST and POLAR spacecraft is beyond the scope of this study and is the focus of a future effort.

4. Summary

We have developed a technique to project high latitude ion flows observed *in situ* at 850 km by the DMSP satellites into dynamic auroral boundary coordinates. All available, high quality, southern hemisphere, F12 and F13 crossings in 1997 and 1998 have been processed to produce statistical representations of net thermal vertical ion flows sorted by geomagnetic activity (Kp) and IMF *By*, resulting in the following observations and conclusions:

1. In agreement with previous research, the most probable flow direction is downward in the PC and upward in the AZ.
2. In agreement with observations on POLAR/TIDE and POLAR/TIMAS, a strong PC upward flow near 9 MLT is observed.
3. There exists a strong dependence of polar cap downward flux location in the polar cap as a function of IMF *By* direction for all Kp, which can be explained by the IMF *By* rotation of the throat of anti-sunward

convection. This effect should be mirrored in the northern hemisphere, i.e. same effect with an opposite *By* relationship.

4. Precipitation boundaries confine upward flowing ions to the AZ under *By* > 0 and less so under *By* < 0.
5. The net flow of ions for all Kp at pre-midnight local times (MLT 20-24) peaks at the PC edge.
6. The net flow of ions for moderate to active Kp [2-9] at post-dusk is enhanced at the AZ equatorward boundary.
7. The pre-midnight enhancement of upward flowing ions seen by DMSP cannot explain dusk energetic outflowing ion observations at 1500-2500km without acceleration processes between 850 and 1500-2500km.
8. The dusk side is more uniformly filled with net flux than the dawn side.

The motivation for developing and applying a dynamic auroral boundary coordinate technique at 850km stems from a need to be able to investigate cold plasma parameters measured *in situ* with respect to precipitating particle energy deposition in a coordinate system that is not sensitive to expansion and contraction of the auroral region. We have used this technique to investigate the influence of IMF *By* on vertical flows and have observed, for the first time, a statistically significant dependence of the

orientation of downward flowing O^+ in the polar cap on the direction of *By*, which can be explained through *By* rotation of the canonical convection cells.

It is beyond the scope of this paper to compare and contrast the O^+ distributions presented here in dynamic coordinates, with fluxes of escaping O^+ obtained in similar coordinates at higher altitudes.

The principal result of this initial investigation is that the auroral boundary does not coincide exactly with the upward/downward flow boundary.

5. Acknowledgements

The authors wish to thank Ed Erwin at the National Geophysical Data Center in Boulder, Colorado for providing a DMSP archive; Tom Sotirelis and Patrick Newell and their Aurora data service at the John's Hopkins University Applied Physics Lab (JHU/APL); Fred Rich of MIT Lincoln Lab for helpful IDM discussions; the THEMIS software team and especially Davin Larson for excellent time series plotting software; Daniel Ober and Ernest Holman from the Air Force Research Laboratory and Boston College respectively for a DMSP noise reduction algorithm; and the Space Physics Interactive Data Resource (SPIDR) for providing IMF values and geomagnetic index quantities. Both referees provided very constructive comments.

6. References

Andersson, L., W. K. Peterson, and K. M. McBryde (2004), Dynamic coordinates for auroral ion outflow, J. Geophys. Res., 109, A08201, doi:10.1029/2004JA010424.

Andersson, L., W. K. Peterson, and K. M. McBryde (2005), Estimates of the suprathermal O^+ outflow characteristic energy and relative location in the auroral oval, *Geophys. Res. Lett.*, 32, L09104, doi:10.1029/2004GL021434.

Andre, M., Yau, A. (1997), Theories and Observations of Ion Energization and Outflow in the High Latitude Magnetosphere, Space Science Review, SSR97.

Chappell, C. R., T. E. Moore, and J. H. Waite Jr. (1987), The ionosphere as a fully adequate source of plasma for the Earth's magnetosphere, J. Geophys. Res., 92, 5896-5910.

Coley, W. R., R. A. Heelis, and M. R. Hairston (2003), High-latitude plasma outflow as measured by the DMSP spacecraft, J. Geophys. Res., 108(A12), 1441, doi:10.1029/2003JA009890.

Cully, C. M., E. F. Donovan, A. W. Yau, and G. G. Arkos (2003), Akebono/Suprathermal Mass Spectrometer observations of low-energy ion outflow: Dependence on magnetic activity and solar wind conditions, *J. Geophys. Res.*, 108(A2), 1093, doi:10.1029/2001JA009200.

Gorney, D., A. Clarke, D. Croley, J. Fennell, J. Luhmann, and P. Mizera (1981), The Distribution of Ion Beams and Conics Below 8000 km, J. Geophys. Res., 86(A1), 83-89.

Greenspan, M. E., Anderson, P. B., Pelagatti, J. M., Characteristics of the thermal plasma monitor (SSIES) for the Defense Meteorological Satellite Program (DMSP) spacecraft S8 through F10, Tech. Rep. AFGL-TR-86-0227, Hanscom AFB, Mass., 1986.

Hardy, D.A. L.K. Schmitt, M.S. Gussenhoven, F.J. Marshall, H.C. Yeh, T.L. Schumaker, A. Huber, and J. Pantazis (1984), Precipitating electron and ion detectors (SSJ/4) for the Block 5D/Flights 6-10 DMSP satellites: calibration and data presentation, AFGL-TR-84-0317, Air Force Geophysics Laboratory, 50 pp., 1984 ADA 157080.

Heppner, J., and N. Maynard (1987), Empirical High-Latitude Electric Field Models, J. Geophys. Res., 92(A5), 4467-4489.

Huddleston, M. M., Chappell, C. R., Delcourt, D. C., Moore, T. E., Giles, B. L., Chandler, M. O. (2005), An examination of the process and magnitude of ionospheric plasma supply to the magnetosphere, J. Geophys. Res., 110, A12202, doi:10.1029/2004JA010401.

Lockwood, M., M. Chandler, J. Horwitz, J. Waite Jr., T. Moore, and C. Chappell (1985), The Cleft Ion Fountain, J. Geophys. Res., 90(A10), 9736-9748.

Loranc, M., W. Hanson, R. Heelis, and J.P. St. Maurice (1991), A Morphological Study of Vertical Ionospheric Flows in the High Latitude F Region, J. Geophys. Res., 96(A3), 3627-3646.

Lotko, W. (2007), The magnetosphere-ionosphere system from the perspective of plasma circulation: A tutorial, Journal of Atmospheric and Solar-Terrestrial Physics, Volume 69, Issue 3, Global Aspects of Magnetosphere-Ionosphere Coupling, Global Aspects of Magnetosphere-Ionosphere Coupling, March 2007, Pages 191-211, ISSN 1364-6826, DOI: 10.1016/j.jastp.2006.08.011.

Meng, C.-I., Kroehl, H. (1977), Intense Uniform Precipitation of Low-Energy Electrons Over the Polar Cap, J. Geophys. Res., 82(16), 2305-2313.

Moore, T. E., and J. L. Horwitz (2007), Stellar ablation of planetary atmospheres, Rev. Geophys., 45, RG3002, doi:10.1029/ 2005RG000194.

Newell, P. T., W. J. Burke, E. R. Sánchez, C.-I. Meng, M. E. Greenspan, and C. R. Clauer (1991), The Low-Latitude Boundary Layer and the Boundary Plasma Sheet at Low Altitude: Prenoon Precipitation Regions and Convection Reversal Boundaries, J. Geophys. Res., 96(A12), 21,013–21,023.

Newell, P. T., Y. I. Feldstein, Y. I. Galperin, and C.-I. Meng (1996), Morphology of nightside precipitation, J. Geophys. Res., 101(A5), 10,737–10,748.

Peterson, W. K., H. L. Collin, O. W. Lennartsson, and A. W. Yau (2006), Quiet time solar illumination effects on the fluxes and characteristic energies of ionospheric outflow, J. Geophys. Res., 111, A11S05, doi:10.1029/2005JA011596.

Peterson, W. K., and E. G. Shelley (1984), Origin of the plasma in a cross-polar cap auroral feature (Theta aurora), J. Geophys. Res., 89(A8), 6729–6736.

Peterson, W. K. (2002), Ionospheric Influence on Substorm Development, Proceedings of the Sixth International Conference on Substorms, University of Washington, ISBN 0-9711740-3-2, p. 143.

Peterson, W. K., L. Andersson, B. C. Callahan, H. L. Collin, J. D. Scudder, and A. W. Yau (2008), Solar-minimum quiet time ion energization and outflow in dynamic boundary related coordinates, J. Geophys. Res., 113, A07222, doi:10.1029/2008JA013059.

Rich, F., and M. Hairston (1994), Large-Scale Convection Patterns Observed by DMSP, J. Geophys. Res., 99(A3), 3827-3844.

Richmond, A. D. (1992), Assimilative Mapping of Ionosphere Electrodynamics, Advances in Space Research, Volume 12, Issue 6, 1992, Pages 59-68, ISSN 0273-1177, DOI: 10.1016/0273-1177(92)90040-5.

Shay, M.A., and M. Swisdak (2004), Three-species collisionless reconnection: Effect of O^+ on magnetotail reconnection, *Phys. Rev.Lett*, 93, 175001, doi:10.1103/PhysRevLett.93.175001.

Shelley, E. G., Johnson, R. G., Sharp, R. D. (1972), Satellite observations of energetic heavy ions during a geomagnetic storm, J. Geophys. Res., 77, 6104-6110.

Sotirelis, T., and P. T. Newell (2000), Boundary-oriented electron precipitation model, J. Geophys. Res., 105(A8), 18,655–18,673.

R. J. Strangeway, R. E. Ergun, Y. Su, C. W. Carlson, and R. C. Elphic (2005), Factors controlling ionospheric outflows as observed at intermediate altitudes, J. Geophys. Res., 110, A03221, doi:10.1029/2004JA010829.

Tung, Y. K., C. Carlson, J. McFadden, D. Klumpar, G. Parks, W. Peria, and K. Liou (2001), Auroral polar cap boundary ion conic outflow observed on FAST, J. Geophys. Res., 106(A3), 3603-3614.

Winglee, R. M., Chua, D., Brittnacher, M., Parks, G. K., Lu, G. (2002), Global impact of ionospheric outflows on the dynamics of the magnetosphere and

cross-polar cap potential, J.Geophys.Res., 107, A9, doi:10.1029/2001JA000214, 2002

Yau, A. W., Abe, T., Peterson, W. K. (2007), The polar wind: Recent observations, JASTP, doi:10.1016.

Yau, A.W., and M. André (1997), Sources of ion outflow in the high latitude ionosphere, Space. Sci. Rev., 80, 1-25, doi: 10.1023/A:1004947203046.

Captions

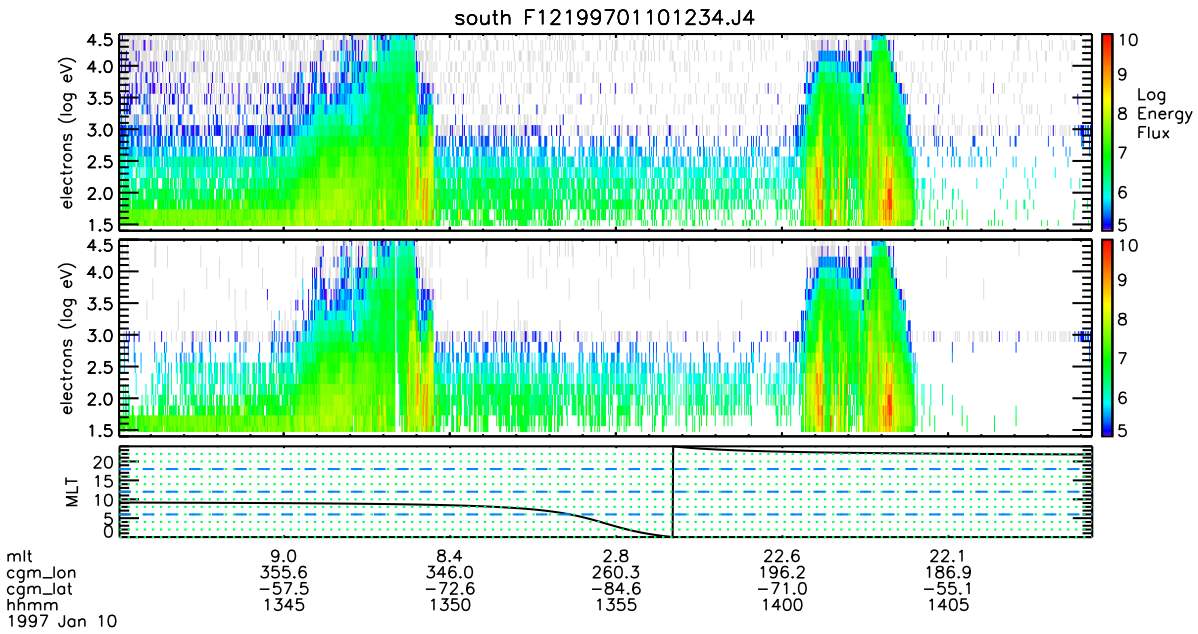

Figure 1: Application of the AFRL background removal technique to precipitating electrons (eV/cm^2/s/sr/eV) for an F12 orbit on January 10, 1997 (same polar crossing as presented in Figure 2). Low count noise from penetrating radiation was removed from the top panel to produce the bottom panel.

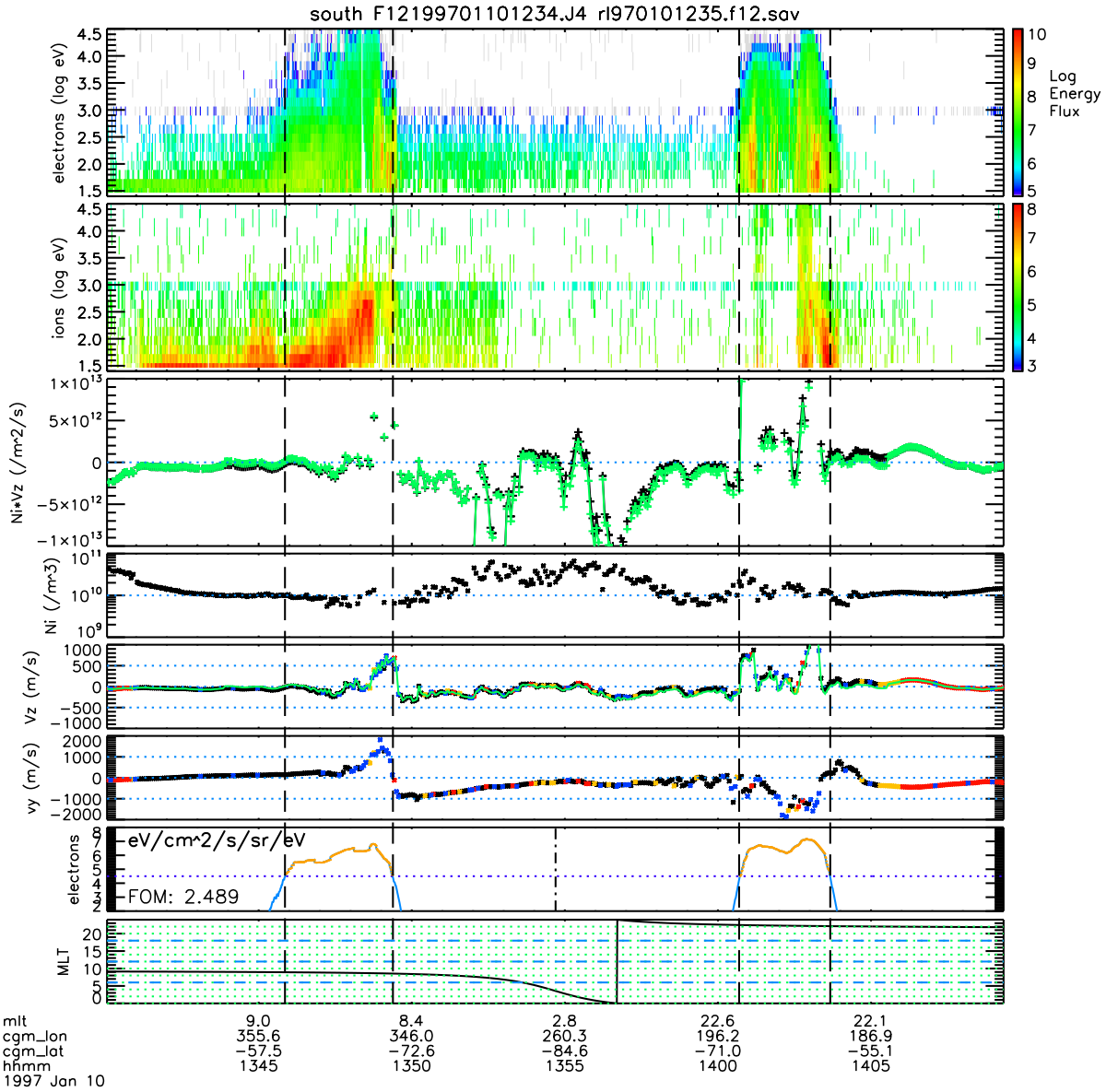

Figure 2: Example of auroral oval identification from high-energy particle precipitation for an F12 orbit on January 10, 1997. From top to bottom, the panels are a) precipitating electrons (eV/cm^2/s/sr/eV), b) precipitating ions (eV/cm^2/s/sr/eV), c) vertical bulk ion number flux (positive spacecraft zenith), d) ion density, e) vertical ion velocity (positive spacecraft zenith), f) horizontal ion velocity (positive sunward), g) high energy electron

precipitation flux (smoothed average) eV/cm^2/s/sr/eV, h) magnetic local time. The figure of merit in g) is used to identify orbits of high quality.

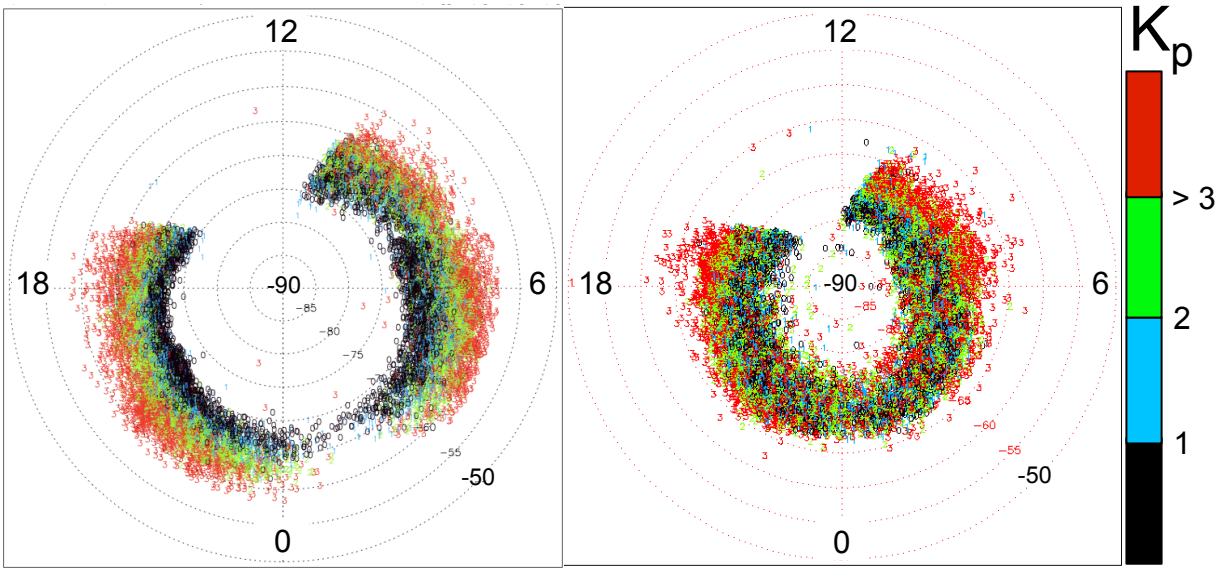

Figure 3: Equatorward (EQ) boundary (left) and Poleward (PC) boundary (right) locations as a function of geomagnetic index Kp (color bar), plotted in magnetic local time and magnetic latitude. 18,772 boundaries from 1997-1998 are shown in each plot.

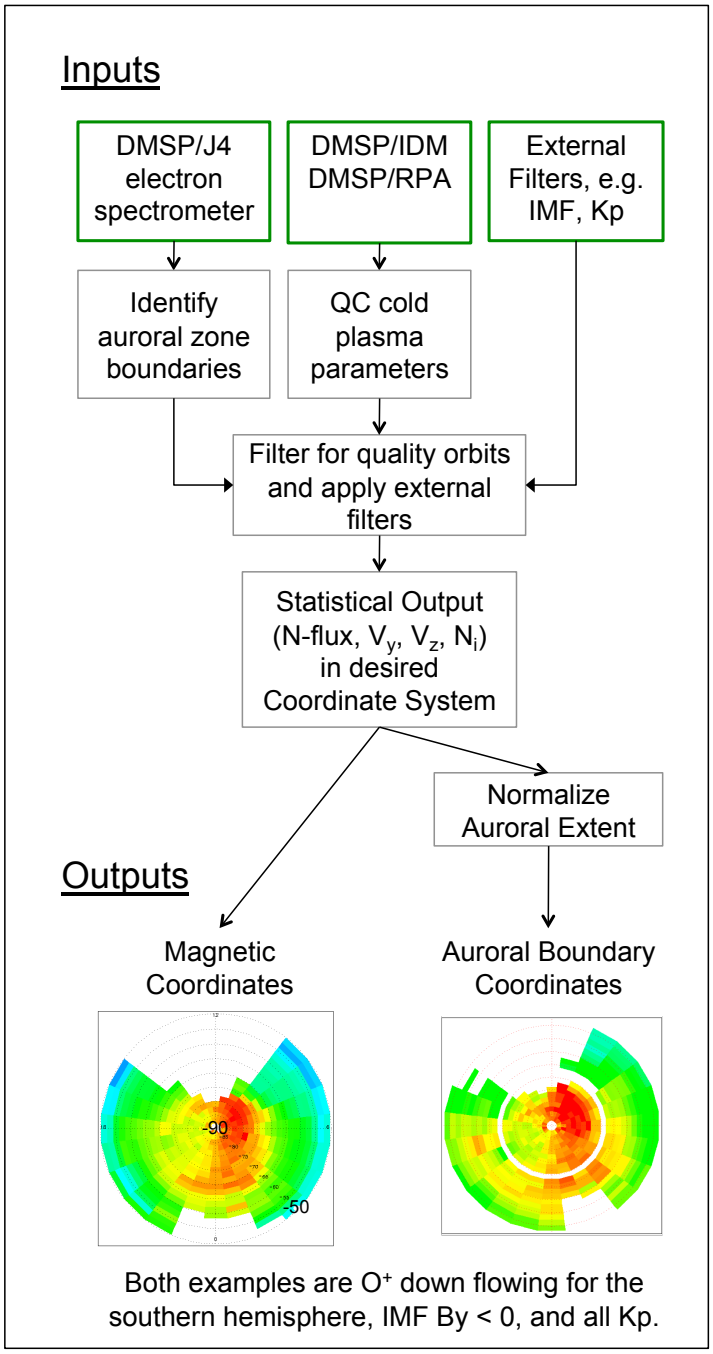

Figure 4: Full procedure: 1) identify auroral zone, 2) quality control cold plasma parameters, 3) filter by geospace condition, 4) create statistical output (e.g. vertical number flux) in chosen coordinate system. The

statistical example shows downward flowing O^+ in magnetic (left) and dynamic boundary (right) coordinates for IMF *By* < 0 and all Kp.

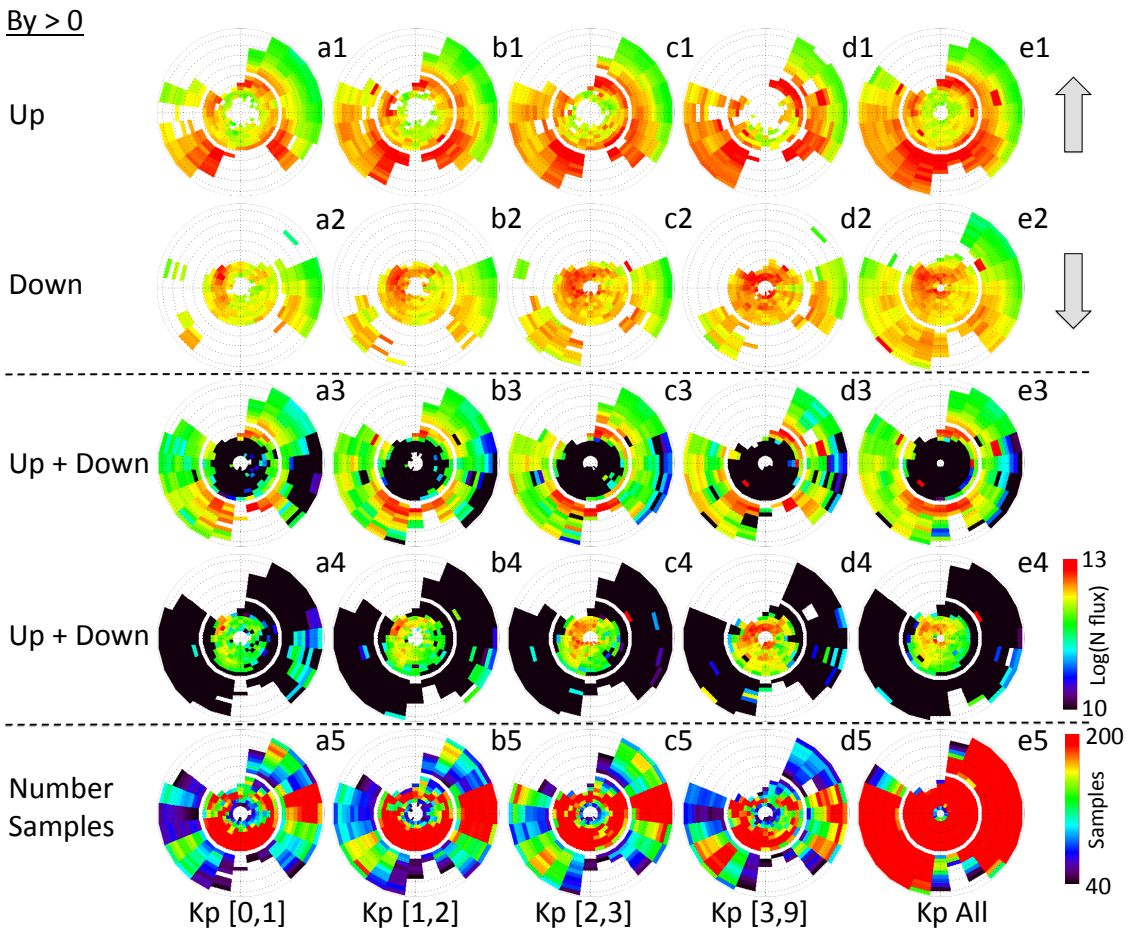

Figure 5: Southern hemisphere vertical ion flows at 850 km in boundary coordinates for IMF *By* > 0 and 5 ranges of Kp. From top to bottom, rows 1-4 represent average flows organized as 1) upward events, 2) downward events, 3) upward + downward (highlighting upward), and 4) upward + downward (highlighting downward). Row 5 depicts the number of samples. From left to right, columns a) – e) represent Kp ranges, organized as: a) Kp

[0-1], b) Kp [1-2], c) Kp [2-3], d) Kp [3-9], e) All Kp. The fluxes in rows 1-4 are plotted with the same scale.

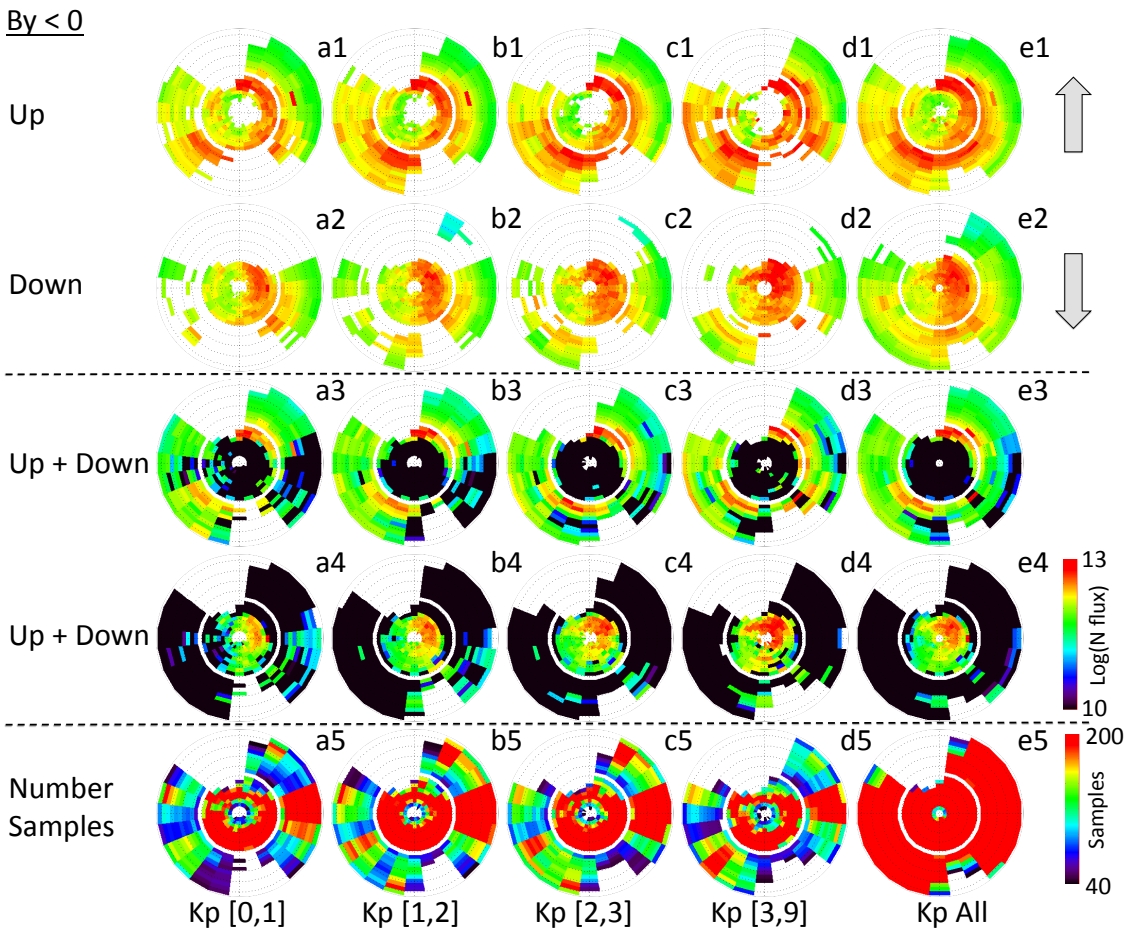

Figure 6: Southern hemisphere vertical ion flows at 850 km in boundary coordinates for IMF *By* < 0 and 5 ranges of Kp. From top to bottom, rows 1-4 represent average flows organized as 1) upward events, 2) downward events, 3) upward + downward (highlighting upward), and 4) upward + downward (highlighting downward). Row 5 depicts the number of samples. From left to right, columns a) – e) represent Kp ranges, organized as: a) Kp

[0-1], b) Kp [1-2], c) Kp [2-3], d) Kp [3-9], e) All Kp. The fluxes in rows 1-4 are plotted with the same scale.

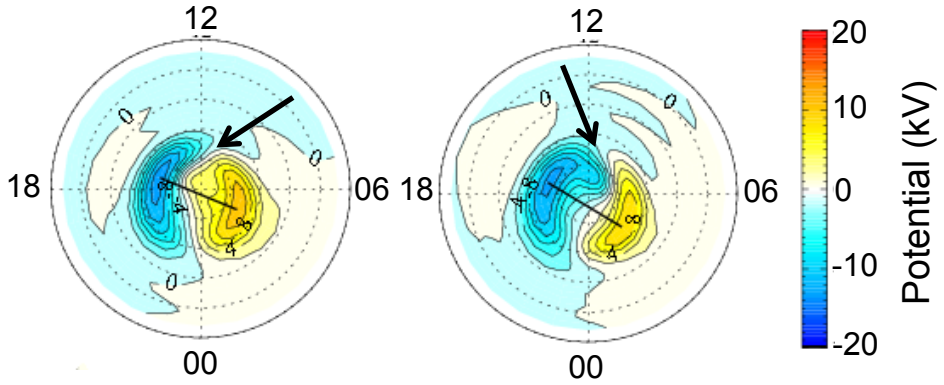

Figure 7: Typical southern hemisphere polar cap potential patterns for IMF *By* > 0 (left) and *By* < 0 (right) using the Assimilative Mapping of Ionospheric Electrodynamics (AMIE) technique. These AMIE data represent the IMF condition 0 < |B| < 5nT and were acquired from NGDC archives of northern hemisphere AMIE output and mapped to the southern hemisphere. Black arrows indicate the orientation of the throat of anti-sunward convection.

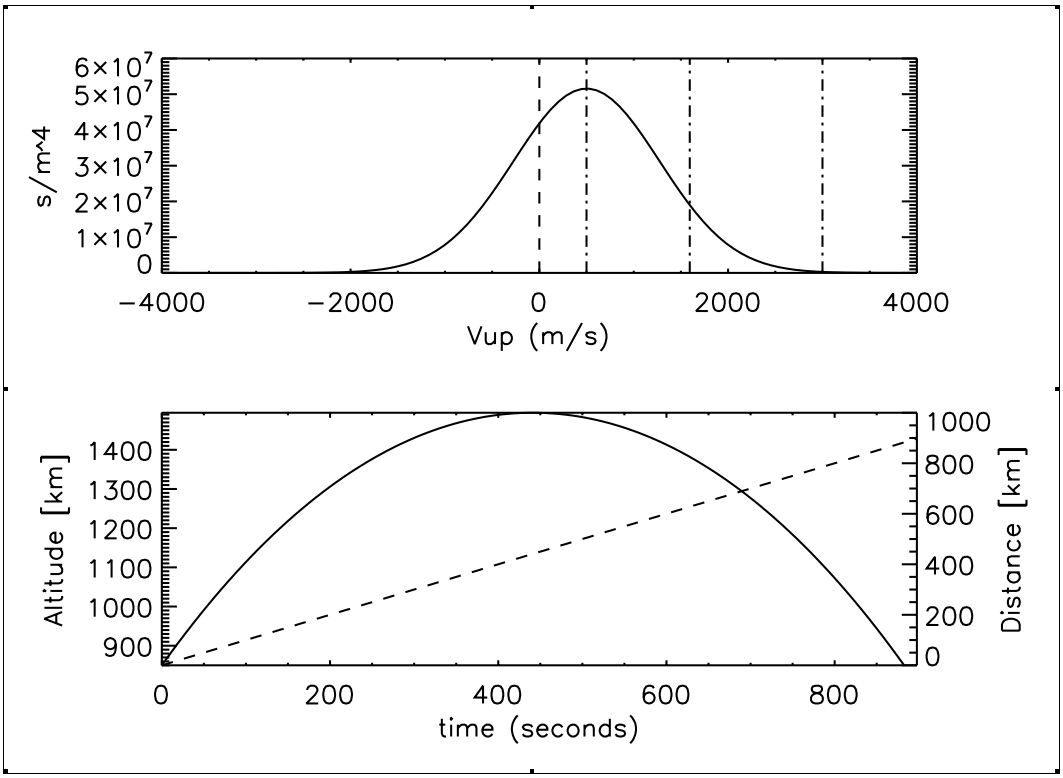

Figure 8: From top to bottom: a) Drifting Maxwellian representing a cold O^+ plasma with temperature of 1160 K (0.1 eV) and drift speed of 500 m/s with vertical markers at 1) 0 m/s, 2) 500 m/s, 3) $500+V_{Thermal}$, 4) $500+2.3V_{Thermal}$ (3000 m/s); b) (left axis) Ballistic trajectory (altitude versus time of flight) with a peak altitude of 1500 km, assuming an upward O^+ flow of 3000 m/s at 850 km altitude, (right axis) Nominal horizontal distance convected during time of flight assuming a transverse flow of 1000 m/s.